Available online at www.sciencedirect.com
ScienceDirect
Journal of Molecular Catalysis A: Chemical 263 (2007) 266–272
JOURNAL OF MOLECULAR CATALYSIS A: CHEMICAL
www.elsevier.com/locate/molcata

The negative effect of residual sodium on iron-based catalyst for Fischer–Tropsch synthesis

Xia An [a,b], Baoshan Wu [a], Wenjuan Hou [a,b], Haijun Wan [a,b], Zhichao Tao [a,b], Tingzhen Li [a,b], Zhixin Zhang [a], Hongwei Xiang [a,*], Yongwang Li [a], Bingfu Xu [c], Fan Yi [c]

[a] *State Key Laboratory of Coal Conversion, Institute of Coal Chemistry, Chinese Academy of Sciences, Taiyuan 030001, PR China*
[b] *Graduate School of Chinese Academy of Sciences, Beijing 100039, PR China*
[c] *Department of Physics, Wuhan University, Wuhan 430072, PR China*

Received 8 July 2006; received in revised form 4 September 2006; accepted 4 September 2006
Available online 8 September 2006

Abstract

The residual sodium means remaining in the catalyst if the catalyst precursor has been insufficiently washed after precipitation of Fe and Cu from their nitrate solutions with sodium carbonate. The effect of such residual sodium on the co-precipitated Fe/Cu/K/SiO_2 catalyst, has been investigated in connection with the characteristics of textural properties, reduction and carburization behavior. Fischer–Tropsch synthesis (FTS) was performed in a slurry-phase continuously stirred tank reactor (CSTR). As revealed by N_2 physisorption, residual sodium acts as a textural inhibitor, resulting in bigger iron phase particle size and smaller surface area. H_2 or CO temperature-programmed reduction (TPR) indicates that residual sodium suppresses reduction of catalysts in H_2 environment and carburization in CO environment. The residual sodium also inhibits the extent of carburization during in situ reduction and poisons the FTS reaction in syngas (H_2/CO = 0.67), as demonstrated by the test of X-ray diffraction (XRD) and Mössbauer spectroscopy (MES). The FTS reaction results indicate that CO conversion decreases markedly and the product distribution shifts to lighter hydrocarbons slightly with increasing residual sodium content.

Keywords: Residual sodium; Fischer–Tropsch synthesis; Iron-based catalyst

1. Introduction

The Fischer–Tropsch synthesis (FTS), which converts coal or natural gas into clean liquid fuels and chemicals, is considered as an effective solution to the problem of finding suitable substitutes for liquid fossil fuels [1]. The use of iron-based catalysts is attractive due to their high FTS activity as well as their water–gas shift (WGS) reactivity, which helps make up the deficit of H_2 in the syngas from modern energy-efficient coal gasifiers [2]. Typical iron-based catalysts contain varying amounts of structural additives, such as silica or alumina, and chemical promoters, such as potassium and copper, known to, for example, increase the overall FTS activity or to facilitate the reduction of iron oxide to metallic iron during activations [3].

In order to improve the catalytic performance of iron-based catalyst, many researchers have studied the effects of some metal promoters, especially alkali metal. The impact of the Group I alkali metals upon the activity of iron catalysts has been obtained at medium pressure synthesis conditions and at the same conversion levels [4]. The results showed that Na and K exhibit much higher WGS rate than the other alkali promoter catalysts. Dry and Oosthuizen [5] found that the basicity increased in the order of Ba, Li, Ca, Na and K for the reduced catalyst, and the amount of methane in FTS decreased as the surface basicity increased. Combination of sodium (Na/Fe = 0.1) with either aluminium (Al/Fe = 0.9) or manganese (Mn/Fe = 0.4) produces stable FTS catalysts with high selectivity for light olefins and concurrently suppresses methane selectivity [6]. Diffenbach and Fauth [7] reported that the Na_2CO_3-precipitated Fischer–Tropsch catalysts prepared at low pH (3.7 and 4.7) showed high olefin selectivity ($C_2^=$–$C_4^=$). Moreover, the activity maintenance of these catalysts are superior to that of the catalysts prepared at higher pH (5.8, 7.6 and 9.8); graphitic carbon deposition occurred to a greater degree on Na_2CO_3-precipitated catalysts prepared at high pH comparative to NH_4OH-precipitated catalysts. Xu et al. [8,9] studied composite catalysts containing

* Corresponding author.
E-mail address: hwxiang@sxicc.ac.cn (H. Xiang).

1381-1169/$ – see front matter © 2006 Elsevier B.V. All rights reserved.
doi:10.1016/j.molcata.2006.09.003

zeolites and Na-rich Fe–Cu Fischer–Tropsch catalysts for the hydrogenation of carbon dioxide. The results suggested that sodium migration from the surface of the F–T catalyst to the zeolite seemed to change the acidity of the zeolite and reduction degree of the Fe catalyst. Komaya et al. [10] also investigated the effects of sodium on the structure and Fischer–Tropsch synthesis activity of Ru/TiO_2. It is demonstrated that Na facilitates the decoration and partial encapsulation of Ru by Ti-containing moieties as a consequence of the formation of sodium titanate.

Almost all reports show that sodium plays a positive role as an alkali promoter for Fischer–Tropsch synthesis [4–10]. Furthermore, most of the investigated catalysts were prepared by the conventional precipitation with sodium carbonate [1–10]. It was difficult to remove the sodium completely from catalyst during the course of washing of the precipitates, and the residual sodium in catalyst may influence its catalytic activity and selectivity greatly. Unfortunately, few studies have been reported on the effect of alkali-metal impurities (e.g. residual sodium in the catalyst) for FTS. It was briefly reported that the Na remaining in the Cu/ZnO-based multicomponent catalyst greatly decreased the activity for the CO_2 hydrogenation to methanol [11]. Jun et al. [12] also studied the effect of residual sodium on the catalytic activity of $Cu/ZnO/Al_2O_3$ in methanol synthesized from CO_2 hydrogenation. The results show that $NaNO_3$ present in calcined catalysts inhibits the interaction of CuO phase with ZnO matrix, thus decreases Cu-dispersion.

Considering residual sodium in the catalyst may be greatly different from promoter sodium, it may affluence the structure, reduction/carburization behavior and FTS performance of the catalysts. In this paper, we report our results obtained from a thorough investigation on the effect of residual sodium on the catalytic behaviors of precipitated $Fe/Cu/K/SiO_2$ catalysts for Fischer–Tropsch synthesis.

2. Experimental

2.1. Catalyst preparation

Catalyst precursors used in this study were prepared by a combination of co-precipitated and spray-dried method. In brief, a solution containing both $Fe(NO_3)_3$ and $Cu(NO_3)_2$ in the desired ratio was added to a continuously stirred tanker together with a sodium carbonate solution. The precipitation temperature and pH were maintained at $80 \pm 1\,^{\circ}C$ and 8 ± 0.1, respectively. The precipitate was washed with deionized water different times, subsequently filtered. A serial of catalysts with different residual sodium content were obtained by controlling washing times. The final cakes were re-slurried in deionized water. Required amounts of potassium carbonate aqueous solution and silica sol solution were subsequently added in to the precipitate and the mixture was re-slurried and spray-dried at 250 °C. The spray-dried catalyst precursors were calcined at 400 °C for 8 h in a muffle furnace. The weight compositions of the four catalysts are $100Fe/5.8Cu/5K/25SiO_2$ with different residual sodium, which were labeled as Na-1, Na-2, Na-3 and Na-4 with the increasing residual sodium. The detailed preparation method can be found elsewhere [13].

2.2. Catalyst characterization

BET surface area, pore volume and the pore size distribution of the catalysts were measured by N_2 physisorption at −196 °C using a Micromeritics ASAP 2500 instruments. The samples were degassed under vacuum at 120 °C for 6 h prior to measurement.

Temperature-programmed reduction (TPR) studies were performed using a mixture gas of 5% H_2/Ar (H_2-TPR) or 5% CO/He (CO-TPR). In H_2-TPR experiment, about 30 mg of catalyst was packed in an atmospheric quartz tube flow reactor (5 mm i.d.). Then the catalyst sample was heated in a flow of 5% H_2/Ar from room temperature to 800 °C at a heating rate of 6 °C/min, and the flow rate of the reduction gas was 40 ml/min in the standard state. Hydrogen consumption was monitored by the change of thermal conductivity of the effluent gas stream. The conditions of CO-TPR experiment are similar to those for H_2-TPR, and the only difference is that a liquefied nitrogen bath was used to remove CO_2 formed during the carbon monoxide reduction.

Powder X-ray diffraction (XRD) patterns of the catalyst samples were carried out on a D/max-RA X-ray diffractometer (Rigaku, Japan) with Cu Kα radiation ($\lambda = 0.154$ nm), operated at 40 kV and 100 mA.

The Mössbauer spectra of catalysts were recorded at room temperature by using a CANBERRA Series 40 MCA constant-acceleration Mössbauer spectrometer (CANBERRA, USA), and a 25 mCi 57Co in Pd matrix.

2.3. Fischer–Tropsch synthesis (FTS) reaction procedures

FTS performances of the catalysts were tested in a 1 dm^3 CSTR. For each test, about 20 g fresh catalyst and 320 g liquid wax were loaded in the reactor. After reduction, the reactor system was adjusted to the required reaction conditions. The detailed description of the reactor and product analysis systems has been given elsewhere [14].

3. Results and discussion

3.1. Textural properties of the catalysts

The BET surface areas and pore volumes of the calcinated catalysts with various residual sodium contents are shown in Table 1. It can be clearly seen that the BET surface area and pore volume of catalysts decrease with the increase of the residual sodium content, and the change in average pore diameter is against this trend. The decrease in BET surface area against sodium content is greater with high sodium content. As an example, Na-4 catalyst shows much lower BET surface area than those of the others. It is probable that residual sodium acts as a textural inhibitor, which leads to an increase in particle sizes. The XRD result in this paper shows the same property. Similar results over $Cu/ZnO/Al_2O_3$ catalysts have also been reported by other researchers [11,12].

Table 1
Textural properties of catalysts with various residual Na contents

Catalysts	Na/Fe (wt/wt)	BET surface area (m^2/g)	Average pore diameter (nm)	Pore volume (cm^3/g)
Na-1	0.05/100	174	6.65	0.29
Na-2	0.85/100	167	6.01	0.25
Na-3	2.98/100	135	6.62	0.22
Na-4	9.94/100	37	14.48	0.13

3.2. Temperature-programmed reduction

The effect of the residual sodium on the reduction and carburization behavior of the catalysts was investigated by H_2-TPR and CO-TPR, respectively. Fig. 1 shows the H_2-TPR profiles of the catalysts with the different residual sodium content. As most of the iron-based catalysts, the reduction process in H_2 occurs in two distinct stages in the temperature range of 250–800 °C. The first stage includes two small peaks corresponding to the transformations of the solid solution CuO → Cu and part of α-Fe_2O_3 → Fe_3O_4. As most literature reported, CuO promoter facilitates the reduction of α-Fe_2O_3 when the two phases are well mixed, resulting in the reduction of α-Fe_2O_3 appears at much lower temperature [15,16]. The second stage represents the transformation of Fe_3O_4 → α-Fe [15–17].

The H_2-TPR profile clearly shows that the first stage reduction peak of catalysts shifts to higher temperature with the increasing of the residual sodium content. That is, the residual sodium in the catalysts inhibits the reduction of α-Fe_2O_3 in H_2-TPR, resulting in an increase in the reduction temperature. Combined with textural property, it may be reasoned that crystallite size affects the reduction behavior. The highest residual sodium-containing sample (Na-4) leads to the poorest dispersion of iron phase crystallite, resulting in smallest surface area, biggest crystallite particles, further highest reduction temperature of the first stage in H_2-TPR. This result was similar to the Song's result [18].

Moreover, the former two reduction peaks of Na-1, Na-2 and Na-3 are almost overlapped, while Na-4 has two segregated small peaks before 400 °C, from which we can deduce that residual sodium suppresses the interaction between copper and iron, resulting in some difficulty in the reduction of a small fraction of α-Fe_2O_3 because of the inefficient contact with the CuO promoter. The presence of residual sodium does not strongly influence the second step reduction corresponding to Fe_3O_4 → α-Fe, probably because thermodynamics and the nucleation of a new crystal structure, and not H_2 dissociation steps, control the reduction rates at these higher temperature [19].

Fig. 2 shows the CO-TPR profiles of the catalysts with the different residual sodium content. There are three peaks in CO-TPR profile for all the catalysts. The first small peak occurring before 300 °C is ascribed to the reduction of α-Fe_2O_3 → Fe_3O_4 [17,20], and the latter two peaks corresponding to the concurrent reduction and carburization of Fe_3O_4 accompanying the Boudouard reaction ($2CO \rightarrow C + CO_2$) [16] are overlap to some extent. We can see that the required temperature of α-Fe_2O_3 → Fe_3O_4 increases with the increase of the residual sodium content. This result is similar to that in H_2-TPR, indicating that residual sodium also suppresses the first stage reduction of α-Fe_2O_3 in CO. It can be seen that the second peak shifts to higher temperature and the areas under the latter two peaks change smaller with the increasing residual sodium, which indicate residual sodium disfavors carburization of catalyst.

3.3. X-ray diffraction study

Fig. 3 is the XRD patterns of the catalysts after calcinations at 400 °C. The major detectable iron phase of the catalysts is

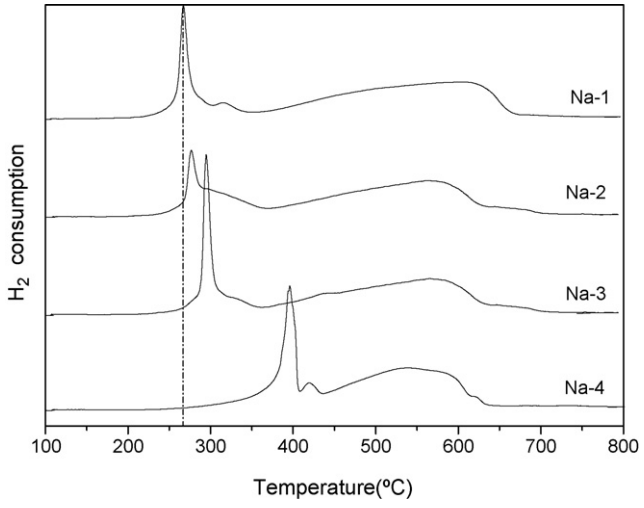

Fig. 1. H_2-TPR profiles of the catalysts.

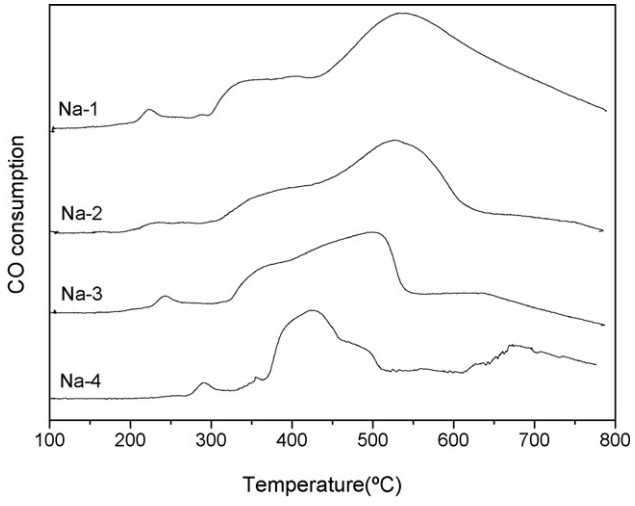

Fig. 2. CO-TPR profiles of the catalysts.

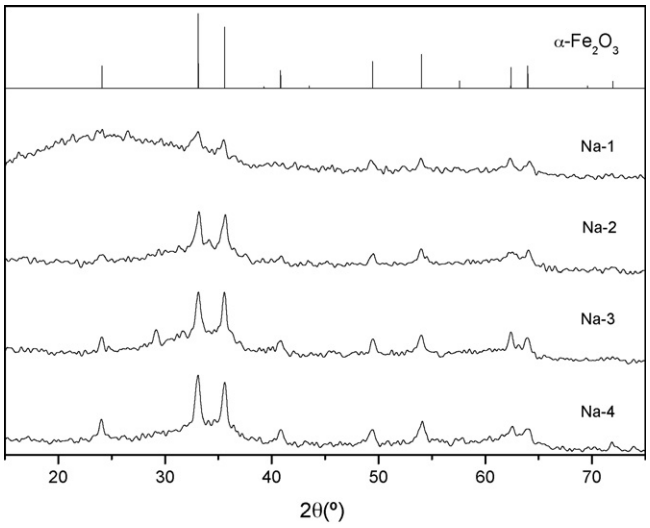

Fig. 3. XRD patterns of the catalysts after calcinations (400 °C).

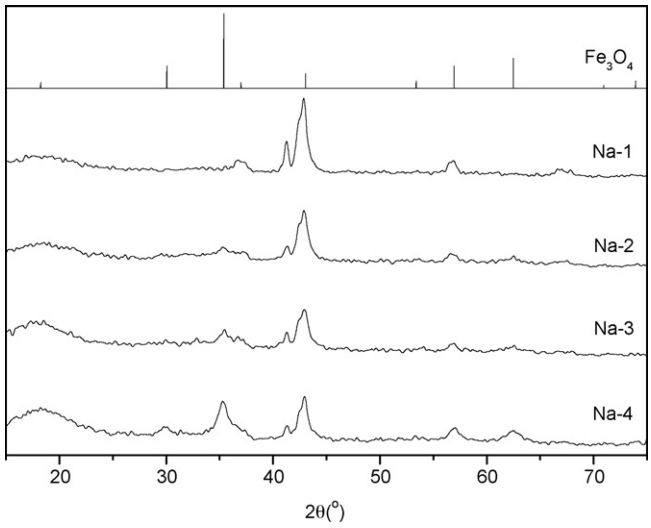

Fig. 5. XRD patterns of the catalysts after reaction.

hematite (α-Fe_2O_3), which has characteristic peaks at 2θ values of 24.2°, 33.1°, 35.6°, 40.8°, 49.52°, 54.0°, 57.6°, 62.5° and 64.0° according to the data reported in the JCPDS. With the increase of the residual sodium content, the characteristic peaks of α-Fe_2O_3 become obviously strong. This result implies that residual sodium in the precipitated Fe/Cu/K/SiO_2 promotes the aggregation of α-Fe_2O_3 crystallite, which is consistent with the observed decrease of the BET surface area.

The XRD patterns of the catalysts with different levels of residual sodium after pretreatment with syngas (H_2/CO = 0.67) at 275 °C, 0.4 MPa and 1000 h^{-1} for 14 h are presented in Fig. 4. The patterns of the catalysts sample after pretreatment have the main peaks of iron carbides or the overlapped peaks of Fe_3O_4 and iron carbides (FeC_x) [21,22], except for Na-4, which has simultaneously the characteristic peaks of unreduced α-Fe_2O_3. Na-4 sample is reduced more difficultly than others. The XRD patterns also indicate that the peak intensity of FeC_x clearly decreases with the increasing of residual sodium content, which demonstrates that residual sodium restrains the reduction and carburization of the Fe/Cu/K/SiO_2 catalysts. This is consistent with the results of H_2-TPR and CO-TPR mentioned above.

The XRD patterns of the samples from catalysts after FTS reaction with syngas (H_2/CO = 0.67) at 250 °C, 1.5 MPa and 2000 h^{-1} for 500 h are presented in Fig. 5, which display somewhat similar variation trend to those after pretreatment. The patterns of all catalysts samples after reaction show the main peaks of iron carbides or the overlapped peaks of Fe_3O_4 and iron carbides. And the peak intensity of FeC_x decreases with the increasing of residual sodium content. The XRD pattern of the catalyst sample Na-4 after 500 h reaction shows clearly the characteristic peaks of Fe_3O_4 as well as that of FeC_x.

3.4. Mössbauer spectroscopy study

Mössbauer spectroscopy was used to give the content of the iron-phase composition quantitatively [23]. Figs. 6 and 7 are the Mössbauer spectra for the catalysts after pretreatment and after 500 h of FTS reactions, respectively. Tables 2 and 3 list the iron-phase composition by fitting the Mössbauer spectra.

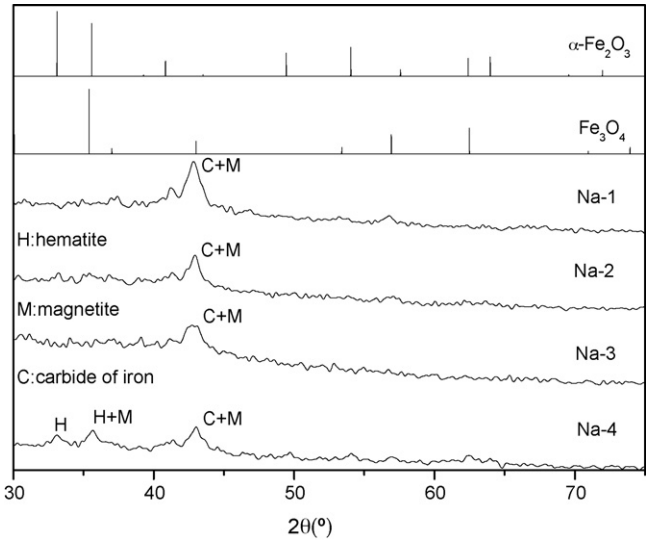

Fig. 4. XRD patterns of the catalysts after reduction.

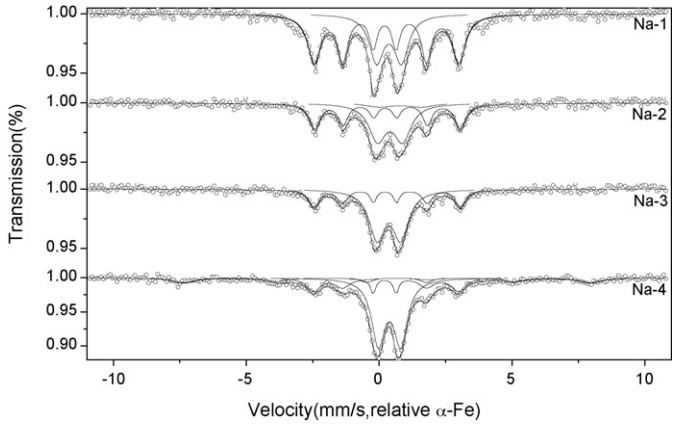

Fig. 6. Mössbauer spectra of the catalysts after reduction for 14 h.

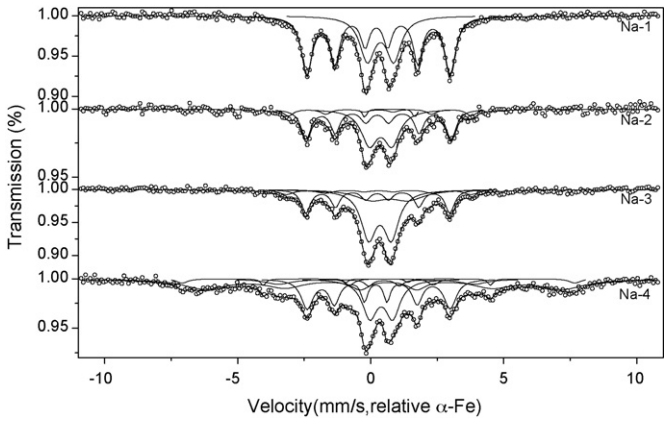

Fig. 7. Mössbauer spectra of the catalysts after reaction for 500 h.

Table 2
Mössbauer parameters of the catalysts after reduction

Catalysts	Phases	MES parameters			
		IS (mm/s)	QS (mm/s)	Hhf (kOe)	Area (%)
Na-1	FeC_x	0.24	0.07	169	66.7
	Fe^{3+}(spm)	0.37	0.93		33.3
Na-2	FeC_x	0.27	0.09	171	45.1
	Fe^{3+}(spm)	0.41	0.94		47.0
	Fe^{2+}(spm)	0.80	1.59		7.9
Na-3	FeC_x	0.26	0.09	172	35.1
	Fe^{3+}(spm)	0.37	0.89		64.9
Na-4	Fe_2O_3	0.45	−0.35	477	15.6
	FeC_x	0.23	0.05	170	25.5
	Fe^{3+}(spm)	0.39	0.84		55.1
	Fe^{2+}(spm)	0.66	2.25		3.8

Reduction conditions: $H_2/CO = 0.67$, 275 °C, 0.4 MPa and 1000 h^{-1} for 14 h.

Table 3
Mössbauer parameters of the catalysts after reaction

Catalysts	Phases	MES parameters			
		IS (mm/s)	QS (mm/s)	Hhf (kOe)	Area (%)
Na-1	FeC_x	0.25	0.08	168	67.0
	Fe^{3+}(spm)	0.37	1.00		33.0
Na-2	FeC_x	0.32	0.05	214	11.1
		0.27	0.05	169	46.7
	Fe^{3+}(spm)	0.37	0.85		39.6
	Fe^{2+}(spm)	0.71	1.88		2.6
Na-3	FeC_x	0.30	−0.01	217	9.8
		0.26	0.03	168	28.0
	Fe^{3+}(spm)	0.35	0.86		43.1
	Fe^{2+}(spm)	0.72	1.40		19.0
Na-4	Fe_3O_4 (A)	0.26	0.06	459	3.9
	Fe_3O_4 (B)	0.58	−0.19	419	34.9
	FeC_x	0.35	−0.30	228	10.1
		0.24	0.11	167	28.1
	Fe^{3+}(spm)	0.39	0.86		20.7
	Fe^{2+}(spm)	0.77	3.15		2.3

Reaction conditions: $H_2/CO = 0.67$, 250 °C, 1.5 MPa and 2000 h^{-1}.

From Tables 2 and 3, it can be seen that the detected iron phases in catalysts after pretreatment and after FTS reaction include α-Fe_2O_3, Fe_3O_4, FeC_x, Fe^{3+}(spm) and Fe^{2+}(spm). Super paramagnetic (spm) refers to iron phases located in small particles with diameter less than 13.5 nm [24], which cannot be well identified at room temperature. The percentage of FeC_x phase in catalysts after reaction as well as after reduction decrease following the order of Na-1, Na-2, Na-3 and Na-4. The results are consistent with what were found in the XRD experiments, indicating that residual sodium inhibits the carburization of the catalysts to some extent. This phenomenon may also be in connection with the textual properties of catalysts with the residual sodium. The bigger crystallites size may disfavor the carburization of the catalysts, e.g. Na-4.

The results obtained from BET and TPR demonstrate the residual sodium on the catalysts leads to bigger crystallite of iron phase, restrains the reduction and carburization of catalysts in pure H_2 and/or CO environment. XRD and MES results show that the catalyst with different residual sodium levels after pretreatment and reaction in sygas ($H_2/CO = 0.67$) can provide different amounts of FeC_x and Fe_3O_4. Combined all these characterization, we expected that they may exhibit different performance in FTS. This speculation is verified by the reaction results in the proceeding sections.

3.5. FTS performance

Typical data of FTS activity, CO_2 selectivity and hydrocarbon distribution of the catalysts are summarized in Table 4. FTS performance of the Fe/Cu/K/SiO_2 catalysts with different residual sodium content was measured under conditions of 250 °C, 1.5 MPa, 2000 h^{-1} and $H_2/CO = 0.67$. At this fixed set of process conditions, CO conversion of the four catalysts is in the range of around 20–51% and monotonously increases with the decreasing residual sodium. Moreover, the hydrocarbon yield also shows similar variation trend. Therefore, it seems that catalyst FTS activity increases with the decreasing residual sodium.

It has been demonstrated that the catalyst activity during FTS is correlated with the formation of active phases. These active phases were formed both in activation process and in FTS reaction. Some researches proposed that the formation of iron carbides were co-related with catalyst activity [25–29]. Iron carbides have been supposed to be the most likely active phases or can have active sites on their surfaces for FTS reactions in recent study [30–33]. Thus the content of FeC_x can be used to monitor the formation of FTS active sites to some extent. Previous XRD and MES studies display that Na-1 has the highest amount of iron carbide both after pretreatment and after FTS reaction. The amounts of iron carbides decrease with the increase of residual sodium. In present experiment, there is a correlation between the carburization extent and the catalytic activity. The higher residual sodium content in the catalyst leads to poorer iron-phase crystallites, resulting in more difficult to reduction and carburization of the catalysts, and subsequently lowers FTS activity.

The WGS activity in the present study is represented by $Kp = P_{CO_2}P_{H_2}/P_{CO}P_{H_2O}$. The extent of WGS reaction decreases with the increase of the residual sodium content. From Table 4,

Table 4
FTS performances of the catalysts with different residual sodium

	Catalyst							
	Na-1		Na-2		Na-3		Na-4	
Time on stream (h)	343	506	319	507	297	511	319	503
CO conversion (x/%)	51.95	51.61	48.45	43.53	42.28	38.10	28.86	17.48
H_2 conversion (x/%)	47.68	48.07	44.40	39.81	44.39	42.97	26.51	17.10
WGS reaction								
$n(H_2)/n(CO)$ in tail gas	0.73	0.72	0.73	0.72	0.65	0.62	0.69	0.67
$n(H_2)/n(CO)$ usage	0.62	0.63	0.62	0.61	0.70	0.76	0.62	0.66
Extent of WGS ($P_{H_2}P_{CO_2}/P_{CO}P_{H_2O}$)	4.42	4.35	4.27	4.67	2.44	1.69	2.89	1.95
CO_2 selectivity (x/%, C basis)	44.78	44.35	43.31	43.88	44.41	42.90	40.32	38.45
HC distribution (wt/%)								
C_1	5.04	4.91	4.45	4.62	6.60	6.78	5.14	4.46
$C_2^=$–$C_4^=$	13.50	13.03	15.23	15.29	16.29	17.39	18.77	16.50
C_2–C_4	17.31	16.73	18.80	18.97	21.57	22.80	22.68	20.19
$C_5^=$–$C_{11}^=$	16.64	16.56	21.71	19.81	23.21	21.82	24.98	25.69
C_5–C_{11}	21.89	21.82	28.98	26.03	31.90	29.32	32.10	33.13
C_{12}^+	55.76	56.54	47.77	50.38	39.93	41.10	40.08	42.22
Olefin selectivity								
$C_2^=/C_2^\circ$	3.63	3.87	3.21	3.23	1.98	2.01	1.31	1.43
$C_3^=/C_3^\circ$	5.16	5.06	5.35	5.13	4.95	5.14	5.69	5.27
$C_7^=/C_7^\circ$	4.38	4.38	3.88	3.77	3.86	4.47	4.07	5.29
Total HC (g/g-cat h)	0.19	0.20	0.18	0.16	0.16	0.15	0.10	0.08

Reaction conditions: $H_2/CO = 0.67$, 250 °C, 1.5 MPa and 2000 h^{-1}.

hydrocarbon distribution of the catalysts can be seen obviously besides WGS and FTS activity. The CH_4 selectivity of the four catalysts is in the range of 3.66–6.78% and there is no clear correlation between the CH_4 selectivity and the residual sodium content, while C_2–C_4 and C_5–C_{11} selectivity increase and C_{12}^+ selectivity decrease slightly with the increase of the residual sodium. The mole ratio of $C_2^=/C_2^\circ$ presents decreasing trends with the increasing residual sodium, and the ratio of $C_3^=/C_3^\circ$ and $C_7^=/C_7^\circ$ changes slightly. That is, residual sodium disfavors hydrocarbon production of high molecular weight with C_{12}^+ product and olefin selectivity. Those factors responsible for the hydrocarbon production of the residual sodium catalysts for FTS remain unidentified. The studies of Wilfried et al. [4] have shown the opposite result over iron catalysts. This discrepancy may be caused by the different sodium addition method in the catalyst. Altogether, relative low content of residual sodium in the catalysts affects the performance slightly, while high content affluences textural properties, reduction and carburization of the catalysts heavily.

4. Conclusion

The residual sodium has significant influences on physicochemical properties of the iron-based catalyst, such as textural properties, reduction and carburization behavior, as well as the catalytic activity and selectivity during FTS performance. The residual sodium leads to an increase in particle sizes, thus acts as a textural inhibitor. The residual sodium restrains the reduction and carburization of catalysts in pure H_2 and/or CO environment. The residual sodium also inhibits the extent of caburization during in situ reduction and FTS reaction in syngas ($H_2/CO = 0.67$). Moreover, there is a clear correlation between the carburization extent and the catalytic activity. CO conversion decreases markedly and the product distribution shifts to lighter hydrocarbons slightly with increasing residual sodium content.

Acknowledgments

The authors gratefully acknowledge the financial support from Key Program of National Natural Science Foundation of China (20590361) and National Natural Science Foundation of Shanxi province (2006021014).

References

[1] L.K. Rath, J.R. Longanbach, Energy Sources 13 (1991) 443.
[2] V.U.S. Rao, G.J. Stiegel, G.J. Cinquergrane, R.D. Srivastava, Fuel Process. Technol. 30 (1992) 83.
[3] H.H. Storch, N. Golumbic, R.B. Aderson, The Fischer–Tropsch and Related Synthesis, Wiley, New York, 1951;
R.B. Anderson, The Fischer–Tropsch Synthesis, Wiley, New York, 1984.
[4] N.H. Wilfried, Y. Zhang, R.J. O'Brien, M. Luo, B.H. Davis, Appl. Catal. A: Gen. 236 (2002) 77.
[5] M.E. Dry, G.J. Oosthuizen, J. Catal. 11 (1968) 18.
[6] J. Abbot, N.J. Clark, B.G. Baker, Appl. Catal. 26 (1986) 141.
[7] R.A. Diffenbach, D.J. Fauth, J. Catal. 100 (1986) 466.
[8] Q. Xu, D. He, M. Fujiwara, Y. Souma, J. Mol. Catal. A: Chem. 120 (1997) L23.
[9] Q. Xu, D. He, M. Fujiwara, Y. Souma, H. Yamanaka, J. Mol. Catal. A: Chem. 136 (1998) 161.
[10] T. Komaya, A.T. Bell, Z.W. Sieh, R. Gronsky, F. Engelke, T.S. King, M. Pruski, J. Catal. 152 (1995) 350.
[11] S. Luo, J. Toyir, M. Takeuchi, T. Watanable, Poster Presentation (P-63), Proceedings of the Fourth International Conference on Carbon dioxide Ultilization, Kyoto, Japan, 1997.

[12] K.W. Jun, W.J. Shen, K.S. Rama Rao, K.W. Lee, Appl. Catal. A: Gen. 174 (1998) 231.
[13] B.S. Wu, L. Bai, H.W. Xiang, Y.W. Li, Z.X. Zhang, B. Zhang, Fuel 83 (2004) 205.
[14] L. Bai, H.W. Xiang, Y.W. Li, Y.Z. Han, B. Zhong, Fuel 81 (2002) 1577.
[15] D.B. Bukur, K. Okabe, M.P. Rosynek, C. Li, D. Wang, K.R.P.M. Rao, G.P. Huffman, J. Catal. 155 (1995) 353.
[16] Y. Jin, A.K. Datye, J. Catal. 196 (2000) 8.
[17] S. Li, A. Li, S. Krishnamoorthy, E. Iglesia, Catal. Lett. 77 (2001) 197.
[18] D.C. Song, J.L. Li, J. Mol. Catal. A: Chem. 247 (2006) 206.
[19] M.J. Tiernan, P.A. Barnes, G.M.B. Parkes, J. Phys. Chem. B 105 (2001) 220.
[20] S. Li, S. Krishnamoorthy, A. Li, G.D. Meitzner, E. Iglesia, J. Catal. 206 (2002) 202.
[21] J. Yang, Y.C. Sun, Y. Tang, Y. Liu, H.L. Wang, L. Tian, H. Wang, Z.X. Zhang, H.W. Xiang, Y.W. Li, J. Mol. Catal. 245 (2005) 26.
[22] M.D. Shroff, D.S. Kalakkad, A.G. Sault, A.K. Datye, J. Catal. 156 (1995) 185.
[23] Y. Yang, H.W. Xiang, Y.Y. Xu, L. Bai, Y.W. Li, Appl. Catal. A: Gen. 266 (2) (2004) 181.
[24] N. Sirmanothan, H.H. Hamdeh, Y. Zhang, B.H. Davis, Catal. Lett. 82 (2002) 181.
[25] J.F. Shultz, W.K. Hall, T.A. Dubs, R.B. Anderson, J. Am. Chem. Soc. 78 (1956) 282.
[26] R. Dictor, A.T. Bell, J. Catal. 97 (1986) 121.
[27] K.R.P.M. Rao, F.E. Huggins, V. Mahajan, G.P. Huffman, V.U.S. Rao, B.L. Bhatt, D.B. Bukur, R.J. O'Brien, Top. Catal. 2 (1995) 71.
[28] L.D. Mansker, Y. Jin, D.B. Burker, A.K. Datye, Appl. Catal. A 186 (1999) 277.
[29] S. Li, G.D. Meitzner, E. Iglesia, J. Phys. Chem. B 105 (2001) 5743.
[30] C.H. Zhang, Y. Yang, B.T. Teng, T.Z. Li, H.Y. Zheng, H.W. Xiang, Y.W. Li, J. Catal. 237 (2006) 405.
[31] K. Sudsakorn, J.G. Goodwin, A.A. Adeyiga, J. Catal. 213 (2003) 204.
[32] T.R. Motiope, H.T. Dlamini, G.R. Hearne, N.J. Conville, Catal. Today 71 (2002) 335.
[33] S. Li, G.D. Meitzner, E. Iglesia, J. Phys. Chem. B 105 (2001) 5743.